Push-pull tracer tests: Their information content and use for characterizing non-Fickian, mobile-immobile behavior

Scott K. Hansen[1,2], Brian Berkowitz[2], Velimir V. Vesselinov[1], Daniel O'Malley[1], and Satish Karra[1]

[1]Computational Earth Sciences Group (EES-16), Los Alamos National Laboratory, Los Alamos, New Mexico, USA, [2]Department of Earth and Planetary Sciences, Weizmann Institute of Science, Rehovot, Israel

Abstract Path reversibility and radial symmetry are often assumed in push-pull tracer test analysis. In reality, heterogeneous flow fields mean that both assumptions are idealizations. To understand their impact, we perform a parametric study which quantifies the scattering effects of ambient flow, local-scale dispersion, and velocity field heterogeneity on push-pull breakthrough curves and compares them to the effects of mobile-immobile mass transfer (MIMT) processes including sorption and diffusion into secondary porosity. We identify specific circumstances in which MIMT overwhelmingly determines the breakthrough curve, which may then be considered uninformative about drift and local-scale dispersion. Assuming path reversibility, we develop a continuous-time-random-walk-based interpretation framework which is flow-field-agnostic and well suited to quantifying MIMT. Adopting this perspective, we show that the radial flow assumption is often harmless: to the extent that solute paths are reversible, the breakthrough curve is uninformative about velocity field heterogeneity. Our interpretation method determines a mapping function (i.e., subordinator) from travel time in the absence of MIMT to travel time in its presence. A mathematical theory allowing this function to be directly "plugged into" an existing Laplace-domain transport model to incorporate MIMT is presented and demonstrated. Algorithms implementing the calibration are presented and applied to interpretation of data from a push-pull test performed in a heterogeneous environment. A successful four-parameter fit is obtained, of comparable fidelity to one obtained using a million-node 3-D numerical model. Finally, we demonstrate analytically and numerically how push-pull tests quantifying MIMT are sensitive to remobilization, but not immobilization, kinetics.

1. Introduction

Field tracer testing is generally expensive to perform, and it is thus desirable to gain as much information as possible by drilling as few wells as possible. This is a key motivation behind the use of so-called *push-pull*, or *single-well injection-extraction* (SWIW) tracer tests, which utilize a single well rather than the multiple wells needed for more traditional cross-well tracer tests. Other substantial benefits of the push-pull tests are that typically their duration is much shorter than that of cross-well tests and tracer mass recovery tends to be higher.

Push-pull tests are performed in the following general way: water spiked with tracer is initially pumped into the well, and then subsequently the pumping direction is reversed, so that water is extracted from the well. The tracer concentration in the extracted water is measured continuously during the extraction, generating a breakthrough curve at the well. Interpretation of push-pull tracer tests is an inverse problem: governing parameters are to be inferred from their impact on a resulting breakthrough curve.

Interpretation methodologies have been devised with an eye to identifying a variety of different parameters, including porosity [*Borowczyk et al.*, 1967], longitudinal dispersion coefficient [*Mercado*, 1966], single first-order decay reaction constants [*Snodgrass and Kitanidis*, 1998; *Haggerty et al.*, 1998; *Schroth and Istok*, 2006; *Huang et al.*, 2010], and first-order decay chain reaction constants [*Boisson et al.*, 2013].

Of closer relevance to the current study, the quantification of various mobile-immobile processes by a push-pull methodology has been considered by a variety of authors. In particular, equilibrium sorption with linear isotherms was considered by *Schroth et al.* [2000], and the aforementioned *Huang et al.* [2010] presented an analytic solution incorporating first-order kinetic mass transfer alongside first-order decay. *Haggerty et al.* [2001] considered mobile-immobile mass transfer inside the multirate mass transfer (MRMT) paradigm.

Gouze et al. [2008b] also considered diffusion into secondary porosity, interpreting results from a push-pull test by means of the continuous time random walk (CTRW). Other authors have considered mobile-immobile behavior stemming from matrix diffusion from a push-pull test isolating a single fracture [*Neretnieks*, 2007; *Doughty*, 2010; *Larsson et al.*, 2013].

For an inverse problem to be made well-posed, the output must be sensitive to the input parameter that one would like to infer, and it must be possible to generate a bijective relationship between input and output (because if multiple parameter values map to the same output, they are not uniquely identifiable based on that output). Aspects of both matters have been considered by past authors. In particular, it has been suggested that similarity of flow paths between the push phase and the subsequent pull phase may render large-scale variability undetectable [*Nordqvist and Gustafsson*, 2002], although this does not appear to have been quantified. *Gouze et al.* [2008a] makes this argument for layered formations, and *Nordqvist and Gustafsson* [2004] indicates the same in single fractures with transmissivity varying in plan view. A related argument (based on the similarity of outbound and inbound times) leads *Schroth et al.* [2001] to argue that equilibrium sorption in the absence of dispersion is not apt to be detected. *Cassiani et al.* [2005] also argues that even when dispersion exists and is reliably characterized, it may not be possible to characterize retardation reliably. Regarding unique identifiability, a number of pairs of distinct processes that may not lead to obviously distinct signals have been noted. For instance, *Lessoff and Konikow* [1997] considered matrix diffusion and drift due to natural gradient and indicated that the two processes may lead to similar signals. Connecting the two issues, *Tsang* [1995] numerically compared push-pull tests featuring mobile-immobile processes in the presence and absence of heterogeneous conductivity fields and found that the resulting well breakthrough curves were relatively similar.

Working in a different vein, *Kang et al.* [2015] consider push-pull tests in highly heterogeneous (fractured) media and aim to calibrate parameters describing path *irreversibility* using a CTRW-like Langevin formulation. Their method is devised in the context of velocity fluctuations imposed heuristically on a purely radial flow field and encoded by single-step correlations of the random walker transition times. This method implicitly assumes that particle outbound and inbound paths are sufficiently different that the step transition times for the two times a particle is at a given distance from the well (on its outbound and inbound journeys) are uncorrelated. This in turn implies a high degree of trajectory hysteresis due to pore-scale dispersion, as one might find in fractured media but not in more homogeneous porous media. Since the CTRW is a general framework, there is actually no obstacle to their scheme being fitted to mobile-immobile behavior in the case of path reversibility (as mobile-immobile mass transfer is a cause of different outbound and inbound effective velocities). However, correlations between transition times would have no physical meaning in this case, and one would simply be fitting a radial CTRW of the sort discussed by *Dentz et al.* [2015]. (We will show in section 4, however, that there is a more elegant approach in this specific case.) *Kang et al.* [2015] also report empirical results supporting the idea that a measure of path reversibility is still observable even in highly heterogeneous media.

Traditionally, well breakthrough curve interpretation implicitly assumes the validity of the radial-coordinate advection-dispersion equation (ADE). Interpretation proceeds either by means of an analytic transport solution in radial coordinates [e.g., *Gelhar and Collins*, 1971; *Haggerty et al.*, 2001], or by numerical discretization based on the radial ADE [e.g., *Lessoff and Konikow*, 1997]. Exceptions include techniques for calibrating first-order reaction rates [e.g., *Haggerty et al.*, 1998], which concern the concentration ratio of two coinjected at any given time, rather than breakthrough curve shape. All interpretation methods that we are aware of which are based on breakthrough curve shape implicitly assume the validity of the radial ADE, with the partial exception of *Kang et al.* [2015], which still is rooted in a Langevin form of the radial ADE.

At the same time, it is well known that tracer transport in aquifers may not be well described by the ADE and its analogs [*Berkowitz et al.*, 2006]. This may have a number of causes. In particular, in a heterogeneous conductivity or transmissivity field, purely radial flow is not to be expected [*Nordqvist and Gustafsson*, 2004; *Lessoff and Konikow*, 1997]. Given flow quasi-reversibility, invalid simplifying assumptions about the flow field may prove harmless. However, to our knowledge this has not previously been established, either theoretically or numerically. Consequently, we are motivated to develop a more general interpretive methodology.

In light of the above, our motivations in this work are several:

1. To characterize the information content of the push-pull test, both with regard to its ability to uniquely quantify mobile-immobile transport and with regard to general transport features which are invisible to it.
2. To develop a conceptual framework that is flow-field-agnostic, which avoids embedding known-invalid assumptions and which can be used to decide questions of parameter identifiability *analytically*.
3. To develop a simple, practical method for quantifying general mobile-immobile transport behavior (e.g., kinetic sorption, transport in dual porosity media, and rock matrix diffusion) based on push-pull test breakthrough curves, which can be used easily for predictive modeling, and to illustrate its use.

To this end, we develop a new interpretive methodology that does away with radial continuum approaches, whether ADE or CTRW-based, to interpretation and instead considers particle transition times between adjacent isochrones for Darcy-scale flow: essentially modeling transport as an abstract, discrete-site 1-D CTRW. This perspective allows us to make statements about what may be invisible (most commonly, the heterogeneous hydraulic conductivity field, or *K*-field), and what is certainly visible (to wit, mobile-immobile behavior). It is shown how to quantify the latter, and a simple subordination technique is presented for modification of an existing model which captures only heterogeneous advection in order to add the mobile-immobile trapping behavior characterized by the push-pull test.

In section 2, we consider general mathematical modeling of mobile-immobile mass transfer processes, including those with a heavy-tailed distribution of single sojourn times in the immobile state. In section 3, we evaluate the assumption of particle path reversibility (i.e., the notion that the outbound and inbound paths traced by any individual particle are the same, which is distinct from Darcy flow reversibility on account of hydrodynamic dispersion) via a numerical parametric study. In section 4, we introduce a new, purely temporal, conceptual approach for formulating push-pull interpretation problems, valid as long as we may assume path reversibility. In section 5 we formulate and demonstrate numerical algorithms based on the new conceptual approach, establishing mathematically that push-pull tests are not sensitive to capture rate. In section 6, we demonstrate the new conceptual and numerical approaches on data collected at the MADE site and show comparable performance of our approach to a more elaborate interpretation technique. In section 7, we summarize our key findings.

2. Mathematical Treatment of Mobile-Immobile Processes

Many subsurface solute transport scenarios are naturally modeled using two spatially coextensive domains, each having its own local concentration, such that those concentrations may be in physical or chemical disequilibrium (i.e., there is a net flux between them at certain locations). So-called mobile-immobile solute transport—that of solute which advects only when it is in one, "mobile," state (or domain) but which can also sometimes be trapped in an "immobile" state from which it is eventually released—is naturally modeled in this way. Mobile-immobile transport models may closely mimic physics, for instance when modeling adsorption, or may be an upscaled approximation, for instance when modeling diffusion into secondary porosity. In either case, define mobile concentration, $c(x,t)$ $[\mathrm{M\,L}^{-3}]$, and immobile concentration, $c_{\mathrm{im}}(x,t)$ $[\mathrm{M\,L}^{-3}]$, where x $[\mathrm{L}]$ and t $[\mathrm{T}]$ are the spatial and temporal coordinates, respectively. Then mobile-immobile behavior may be captured by the following set of equations:

$$\frac{\partial c}{\partial t}(x,t)+\frac{\partial c_{\mathrm{im}}}{\partial t}(x,t)=F\{c\}(x,t)$$

(1)

$$\frac{\partial c_{\mathrm{im}}}{\partial t}(x,t)=G\{c,c_{\mathrm{im}}\}(x,t),$$

where F is a linear differential operator representing some combination of advection, dispersion, and decay, and G is an arbitrary operator. In the common case of first-order kinetic mass transfer [*Fetter*, 1999, p. 133],

$$G\{c,c_{\mathrm{im}}\} \equiv \lambda c - \mu c_{\mathrm{im}}.$$

(2)

Here λ $[\mathrm{T}^{-1}]$ represents the probability per unit time that a mobile particle will become immobile, and μ $[\mathrm{T}^{-1}]$ represents the probability per unit time that an immobile particle will become mobile. This implies the following exponential probability distributions for the length of single sojourns in both the mobile state, $\psi_{\mathrm{m}}(t)$ $[\mathrm{T}^{-1}]$, and the immobile state, $\psi_{\mathrm{im}}(t)$ $[\mathrm{T}^{-1}]$:

$$\psi_m(t) = \lambda e^{-\lambda t}, \tag{3}$$

$$\psi_{im}(t) = \mu e^{-\mu t}. \tag{4}$$

However, in some cases, a nonexponential distribution is applicable for single sorption times [*Drazer et al.*, 2000; *Haggerty and Gorelick*, 1995]. In these cases, an alternative expression for G (which we call G^*), previously employed by *Margolin et al.* [2003] can be used

$$G^*\{c\} \equiv \lambda c - \lambda \int_0^t \psi_{im}(\tau) c(x, t-\tau) d\tau. \tag{5}$$

As in (2), λ is a spatially homogeneous probability per unit time that a mobile particle will become immobile, and $\psi_m(t)$ remains as in (3). However, here, the form of $\psi_m(t)$ is defined to be arbitrary. When $\psi_{im}(t)$ is defined as in (4) then G^* collapses to G, so this is a pure generalization of the standard form (2). Substituting G^* as defined in (5) for G in (1) leads to the integrodifferential equation

$$\frac{\partial c}{\partial t}(x, t) = F\{c\}(x, t) - \lambda c(x, t) + \lambda \int_0^t \psi_{im}(\tau) c(x, t-\tau) d\tau. \tag{6}$$

To model transport predictively, it is necessary to characterize the mobile-immobile trapping behavior via λ and ψ_{im}, as well as F, the transport operator that would apply in the absence of any mobile-immobile processes. We will see below that the nature of F is essentially invisible to push-pull tracer tests. However, there is a positive perspective on this: it means push-pull tracer tests are solidly positioned to isolate and to characterize mobile-immobile processes because the well breakthrough data may not be influenced by flow-field heterogeneity.

A potentially useful way to understand the results herein is in the framework of anomalous, or non-Fickian, transport. For our purposes, we distinguish two distinct types of anomalous transport: diffusion-driven and advection-driven. Diffusion-driven anomaly is caused by some sort of trapping process where the capture rate and capture time are *unrelated* to the advection velocity; capture is ultimately driven by molecular diffusion. Assuming a spatial homogeneity of trapping sites, the mobile-immobile processes we seek to characterize—kinetic sorption, matrix diffusion, diffusion into secondary porosity—all fall into this category. By contrast, advection-driven anomaly refers to highly asymmetric breakthrough curves caused by a distribution of velocities among streamlines, such that different particles make different amounts of progress in a given time. Advection-driven anomaly is *related* to the advection velocity, and may also, under flow quasi-reversibility go undetected by a push-pull test.

3. Can We Assume Path Reversibility?

Consider the velocity field generated by a point injection in a confined aquifer. By linearity of the groundwater flow equation, scaling the injection rate by some fixed multiple, m, scales the velocities everywhere by m, without changing their orientation. This shows that regardless of the hydraulic conductivity field, if there are no dispersive processes and the aquifer responds instantaneously to head changes, then all particles released at a given instant will reconvene at the well simultaneously during the pull phase. This means, mathematically, that the operator F in (6) is invisible. As mentioned in the introduction, tracer path reversal has been remarked upon by previous authors [e.g., *Nordqvist and Gustafsson*, 2002], and the last-in-first-out assumption that it entails underpins all push-pull interpretation theory of which we are aware. Nevertheless, it does not appear to have been systematically investigated in light of hydrodynamic dispersion. Consequently, we first examine path reversal before proceeding to further theoretical development that depends on it.

3.1. Assessing the Path Reversal Assumption Under Nonideal Conditions

We performed a computational parametric study to quantify the impact of three natural processes which might combine to interfere with path reversibility: ambient background flow, K-field heterogeneity, and local-scale dispersion. The parametric study involved 100 realizations of 50 m by 50 m, multi-Gaussian, isotropic 2-D log hydraulic conductivity fields were generated, with constant conductivities assigned to each cell a 100 by 100 grid. The fields were generated in MATLAB, using Fourier series methods. All realizations assumed an exponential semivariogram with a correlation length of 4 m, and a geometric mean hydraulic
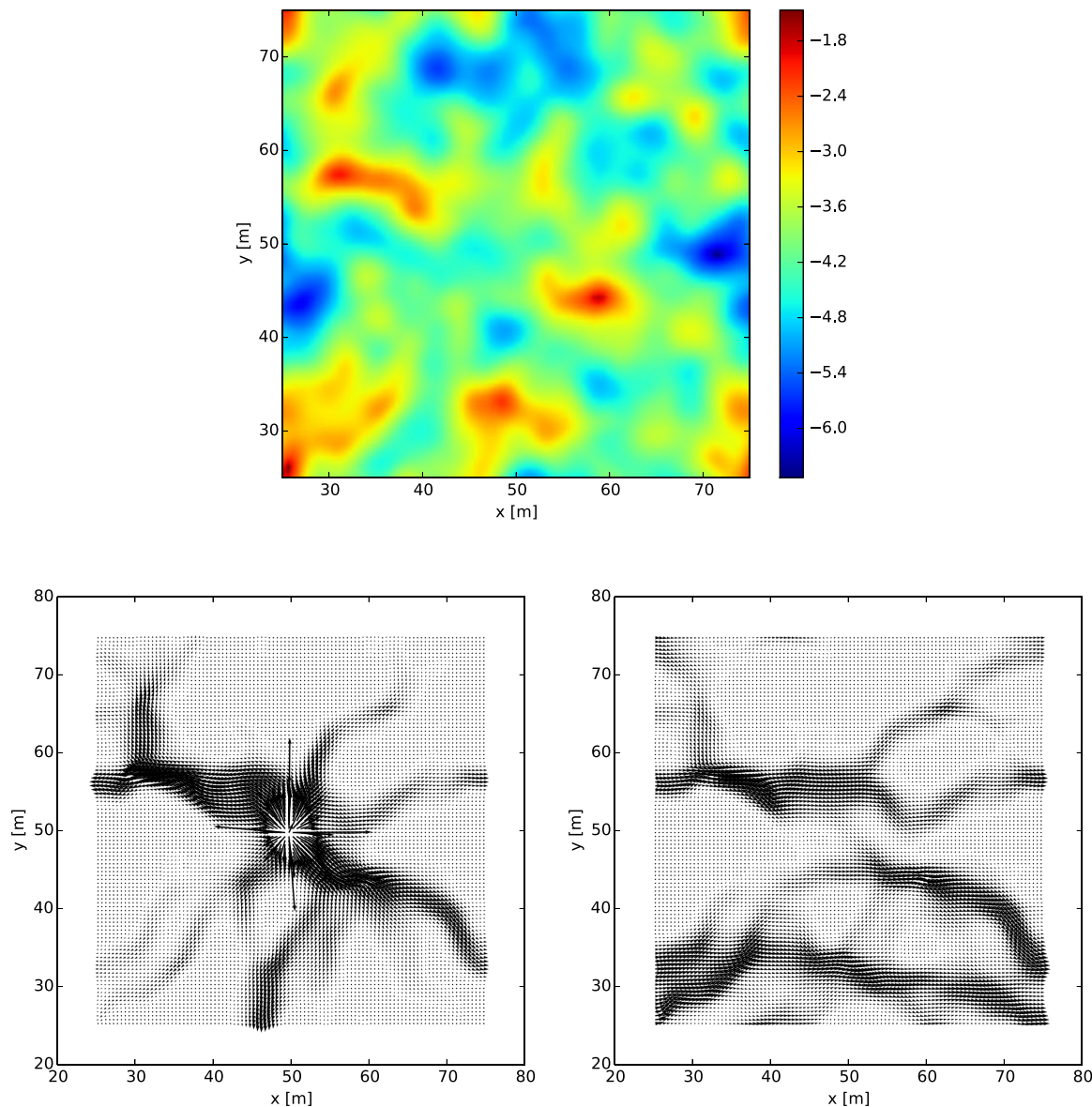
Figure 1. (top) Heat map showing $\log_{10}(K)$ for a single realization from the parametric study, with $\sigma^2_{\ln K} = 1.5$. (bottom) Cell-center velocities calculated by PFLOTRAN using this realization (vectors point in direction of flow and their length is proportional to speed). Flow maps are shown for mass injection at the center (left), and west-to-east ambient flow (right). All diagrams are shown in map view.

conductivity of 10^{-4} m s^{-1}. The realizations were divided into batches of 25, each batch featuring a different value of $\sigma^2_{\ln K}$, respectively 0.5, 1.0, 1.5, and 2.0.

An example hydraulic conductivity field is shown in Figure 1. For each conductivity field, we ran two simulations in PFLOTRAN [*Lichtner et al.*, 2015]. For the first (quasi-radial) simulation, we imposed a constant *mass* injection rate, $Q_{in} = 1$ kg s^{-1}, at the center, and zero head at all points on the outer boundary. For the second (quasi-linear) simulation, we imposed no-flow boundary conditions on the north and south faces (i.e., at $y = 25$ m and $y = 75$ m), and constant head values, higher at the west edge ($x = 25$ m), and lower at the east ($x = 75$ m). In both cases, steady-state velocity fields were computed for each (one vector for each cell on the 100 by 100 grid). These velocity fields were used to simulate push-pull tests under a variety of conditions. For each realization, nine push-pull simulations were performed, exploring each combination of average ambient drift velocities, $v_a = $ of 0, 0.05, and 0.1 m d^{-1}, and longitudinal local-scale dispersivities, $\alpha_l = 0.01$, 0.055, and 0.1 m. In all cases, transverse local-scale dispersivity, $\alpha_t = \alpha_l/10$. The parameter ranges

were chosen so as to be in plausible ranges for a sandy aquifer. The characteristic pore-scale dispersivities were chosen based on the reported ranges in *Schulze-Makuch* [2005] and drift velocity was selected to interpolate between zero and the relatively rapid flow observed at the Borden aquifer [*Mackay et al.*, 1986]. Particle tracking was also run with no drift *and* no pore-scale dispersivity, which confirmed path reversal and instantaneous reconvention of particles in the case of pure advection in the heterogeneous flow field.

The particle tracking code was written in the Julia language, and employed constant, small time steps of duration 0.01 h. For each particle, at each time step, the velocity field was interpolated based on the particle's starting location. If the particle was presently mobile at the start of the time step, it advected along its local streamline for the entire duration of the time step, and then underwent a small random Fickian dispersive motion determined by α_l, α_t, and the streamline velocity. If the particle was immobile at the start of the time step, it was not moved. All particles were injected in the mobile state. If mobile-immobile mass transfer was turned on, at time 0, and each time the particle made a mobile/immobile state transition, the time of the next state transition was selected by making a draw from ψ_m or ψ_{im}, as appropriate. Discussion of other approaches to particle tracking with flow field heterogeneity and potential mobile-immobile mass transfer can be found in *Michalak and Kitanidis* [2000] and *Salamon et al.* [2006] and references therein. The velocity fields were used in the following way during the push-pull simulations on each realization: during the push phase, the velocity fields from the quasi-radial PFLOTRAN simulation were used directly. During the pull phase, these were scaled by a multiple of −1. Ambient drift was simulated for each realization by scaling the velocity vectors of the quasi-linear case so that the mean west-to-east velocity was as desired. Using the principle of superposition, these vectors were added to the vectors obtained from the quasi-linear simulation, and this sum defined the cell-center velocity for each cell.

Particle tracking proceeded by introducing 5000 particles in a ring of diameter 15 cm around the injection location at the center of the domain, and tracking them during a push phase of 40 h, and then through a 200 h pull phase, or until all particles had reconvened at the well. No processes other than local-scale dispersion and advection affected the particles. Since tracer from the tests was found to only interrogate the area immediately surrounding the well (e.g., see Figure 6), the no-flow boundary conditions imposed at the north and south edges of the domain for the quasi-linear simulations were not considered to be relevant.

For each of the nine particle tracking simulations on each of the 100 realizations, the variance and the moment coefficient of skewness (MCS) of the breakthrough curves were computed. The separate averages of the variance and MCS were taken over the 25 realizations in each batch, for each of the nine combinations of drift velocity and local-scale dispersivity. Contour plots of these quantities are shown in Figure 2.

Under perfect path reversibility, as discussed, all the particles which departed the well at the same instant would reconvene at the same instant. This is to say, the well breakthrough curve under such conditions would be a translated Dirac delta function, $\delta(t-80\,\mathrm{h})$, whose central moments are all zero. Based on the fact that the variance is in some places significantly positive (with a standard deviation greater than 10 h found, even in the no-drift case, compared to a mean breakthrough time of 80 h) we see that the path reversibility assumption is only an approximation for push-pull tests in real media. Detectable scattering can emerge from the interaction of local-scale dispersion and flow-field heterogeneity, even in the absence of ambient drift. Fortunately, pore-scale dispersivity can be estimated form core samples, and ambient drift can be estimated from point dilution tests. Thus, it is possible for practitioners to use our results to estimate a degree of likely scattering before a push-pull test is performed.

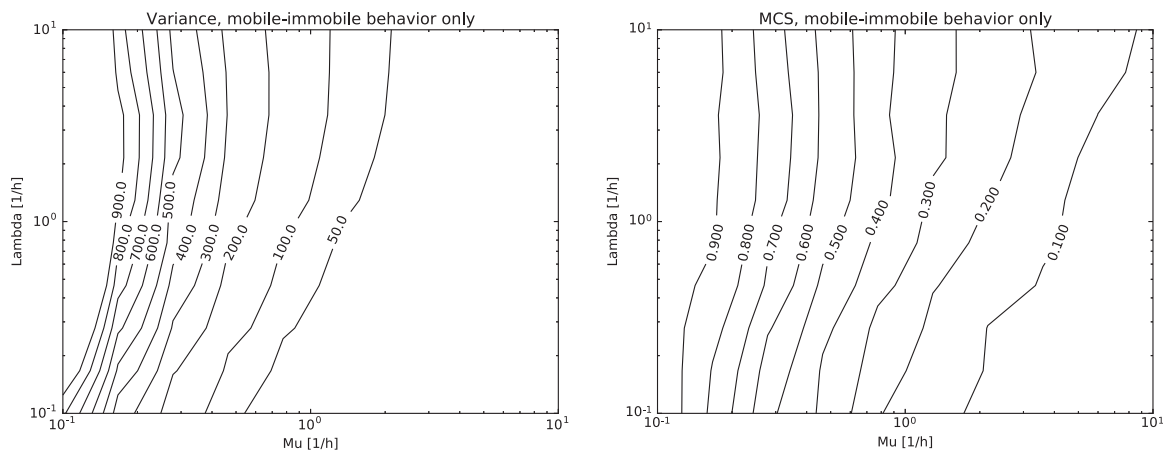### 3.2. Assessing Scattering Due to Mobile-Immobile Mass Transfer

A second study was performed which followed the same methodology, using a single *K*-field realization. This study involved no drift or pore-scale dispersivity (and thus featured total path reversal, with all particles converging at the same instant in the absence of mobile-immobile trapping behavior). It considered the effect of mobile-immobile trapping behavior alone on particle scattering, with a goal of identifying regions of parameter space in which (a) scattering due to mobile-immobile mass transfer dominates the other sources identified above and (b) non-Fickian behavior (i.e., heavy-tailed breakthrough curves that cannot be explained by a constant dispersion obeying Fick's law) is apparent. For simplicity of parameterization, we restricted our study to first-order kinetic mass transfer (2) and did not explicitly consider other forms of ψ_{im}. This appears to be conservative, as it is reasonable to believe that power-law ψ_{im} will generate a stronger signal than exponential ψ_{im}. A range of possible values of λ and μ, the probabilities per unit time that
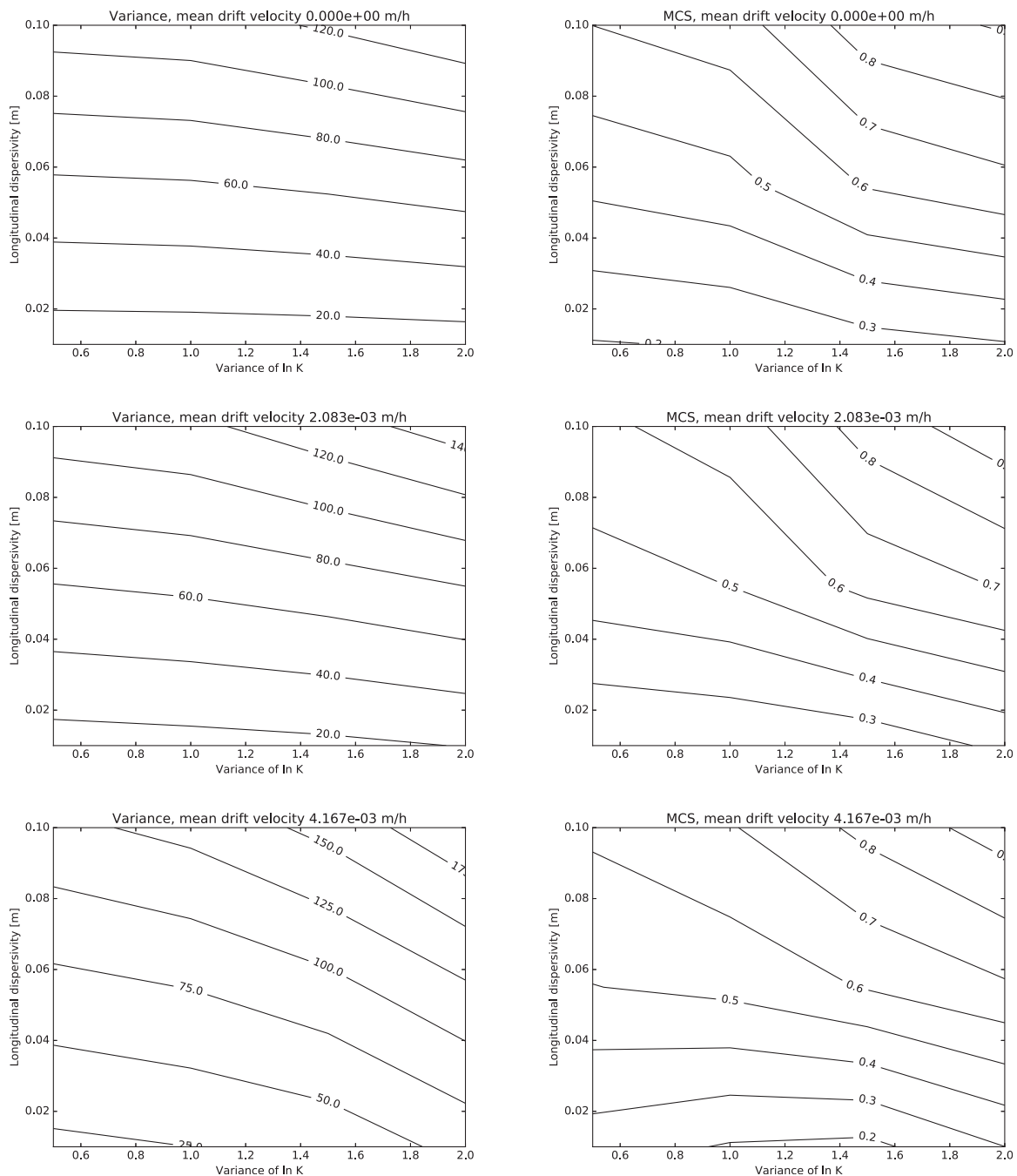
Figure 2. Contour plots quantifying scattering due to interplay of ambient flow, local-scale dispersion, and heterogeneity. Each plot shows a relationship between local-scale dispersivity and K-field heterogeneity. Each row corresponds to a different ambient flow velocity. The left column displays variance and the right column displays moment coefficient of skewness.

mobile and immobile particles will respectively become immobile and mobile, were considered. Bounds were placed on the parameter space based on the fact that particles should be expected to experience multiple immobilization-remobilization cycles during the test (so λ and μ cannot be too small), and the fact that, per *Hansen* [2015], Fickian behavior is expected for $t > 70/\min(\lambda, \mu)$ (so λ and μ cannot be too large).

Contour plots of the variance and MCS of the breakthrough curves as a function of λ and μ were computed and are shown in Figure 3. In order for the assumption of path reversibility to be harmless, it must be true that scattering (for which breakthrough time variance is a proxy) due to hydrodynamic processes is much weaker than scattering due to mass transfer. Furthermore, if we are interested in making inferences about

Figure 3. Contour plots quantifying scattering due to mobile-immobile mass transfer, as a function of λ and μ, as quantified by breakthrough curve variance (left) and moment coefficient of skewness (right).

the mobile-immobile mass transfer by interpreting the heavy tails of the breakthrough curve, the skewness (of which the MCS and variance are together a proxy) due to hydrodynamic processes must be much weaker than the skewness due to mass transfer. It is clear from examining the variance and MCS at different points in v_a-α_Γ $\sigma^2_{\ln K}$ space in Figure 2, in parallel with the variance and MCS at different points in λ-μ space in Figure 3, that this is not generally true.

However, it is apparent from both plots in Figure 3 that the most likely region for identifying a strong and non-Fickian signal in the data and being able to disregard imperfect path reversal lies in the region $\mu \leq 0.4$, $\lambda \geq 1$. In this region, we see that the variance and third central moment of breakthrough due to mobile-immobile behavior are in almost all cases an order of magnitude or more larger than that due to the interaction of ambient drift, local-scale dispersion, and heterogeneity for all the combinations of parameters considered, rendering the assumption of path reversal reasonable. We also note that, in this region, λ has a limited impact on the low-order spatial moments of the breakthrough curves, and μ has a comparatively much larger impact. (We will later show mathematically that as long as λ^{-1} is much shorter than the timescale of the test, push-pull tests actually contain negligible information about λ and that this indifference is not limited to certain spatial moments or to specific parameter values chosen.)

3.3. Visualizing Simultaneous Action of Mobile-Immobile Mass Transfer and Local-Scale Dispersion

The analysis immediately preceding has suggested that, at least in many circumstances, scattering due to hydrodynamic processes will be negligible relative to those of mobile-immobile mass transfer, and it may be reasonable to assume that mobile-immobile mass transfer is the only operative process when interpreting push-pull tests. The hydrodynamic and mobile-immobile mass transfer causes of scattering factors were analyzed separately, respectively in sections 3.1 and 3.2. This is a conservative assumption, since when mass is immobile, it will not undergo any hydrodynamic scattering—however, it may be useful to visualize their simultaneous effect. To that end, we presently introduce what we shall term our *canonical example*: a system with parameters that might be realistic for a push-pull test in a sandy aquifer, for which it would be reasonable to assume path reversal and attempt to quantify mobile-immobile mass transfer. We shall return to this example repeatedly over the next sections, altering specific features to illustrate particular concepts. Note that unlike the preceding parametric study, we do not presume to rest general claims about push-pull behavior on this single example. Rather, we seek to demonstrate the theoretical claims that we make about the information content of push-pull tests and the numerical methods we develop, and to visualize behavior.

The canonical example has the following attributes:

1. Its domain is a heterogeneous hydraulic conductivity field (varying only in map view, defined by an isotropic Gaussian semivariogram with correlation length of 2 m, geometric mean hydraulic conductivity 10^{-4} m s^{-1}, and $\sigma^2_{\ln K} = 2$) on a domain 50 m square in map view and 10 m deep.
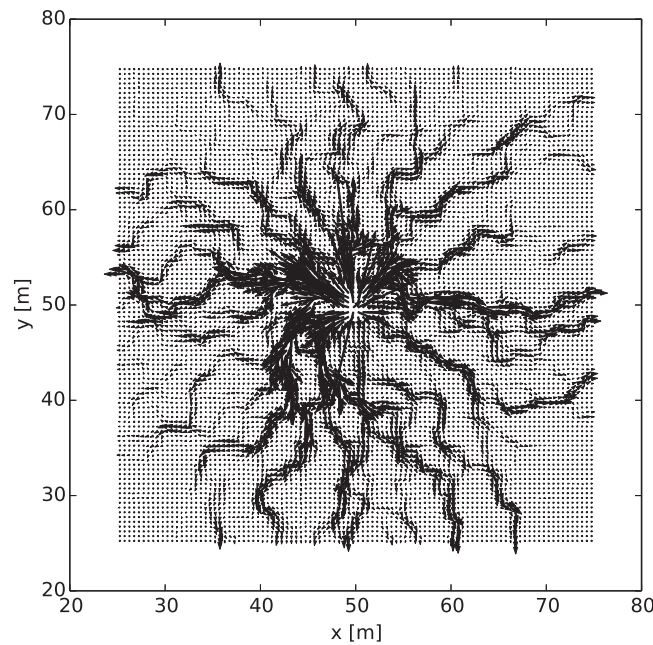
Figure 4. Cell-center velocity field computed by PFLOTRAN during push phase for the canonical example. Diagram is in map view; vectors point in direction of flow and their length is proportional to speed.

2. A push-pull test is simulated in this conductivity field, assuming the aquifer is confined and there is a fully-penetrating well at the center of the map. This is done by solving the groundwater flow equation in PFLOTRAN, assuming negligible storativity (i.e., instantaneous response to changes in head at the well). The Darcy velocity field during the push (injection) phase is shown in Figure 4. Identical rates of injection, Q_{in} [$M\,T^{-1}$], and extraction, Q_{ex} [$M\,T^{-1}$] are used, with $Q_{in} = Q_{ex} = 1$ kg s^{-1} (note that Q here represents a *mass* flow rate).

3. There is no ambient flow. (Having characterized its effect above in the parametric study, we will follow the example of all other analyses of push-pull tests we are aware of in the literature and assume it is zero in the remainder of this document.)

4. The push phase is simulated for 40 h, after which the pull (extraction) phase immediately commences and runs for another 160 h.

5. Moderate local-scale dispersion with $\alpha_l = 1$ cm and $\alpha_t = 0.1$ cm is taken to be operative.

6. First-order kinetic trapping is operative, and in a region of parameter space which will lead to observable tailing. We assume ψ_m exponential, with $\lambda = 10\,h^{-1}$, and ψ_{im} exponential, with $\mu = \frac{1}{3}\,h^{-1}$.

To illustrate the combined effect of mobile immobile mass transfer, local-scale dispersion, and *K*-field heterogeneity, we compare in Figure 5 the breakthrough curve from the canonical example (which features all of these), and the breakthrough curve that would be generated by the canonical example, except with zero local-scale dispersion. The curves in this figure were each generated by tracking 10^5 particles and applying kernel density estimation. The comparatively mild effect of pore-scale dispersion, particularly in the tail region, even on this comparatively heterogeneous conductivity field, is notable.
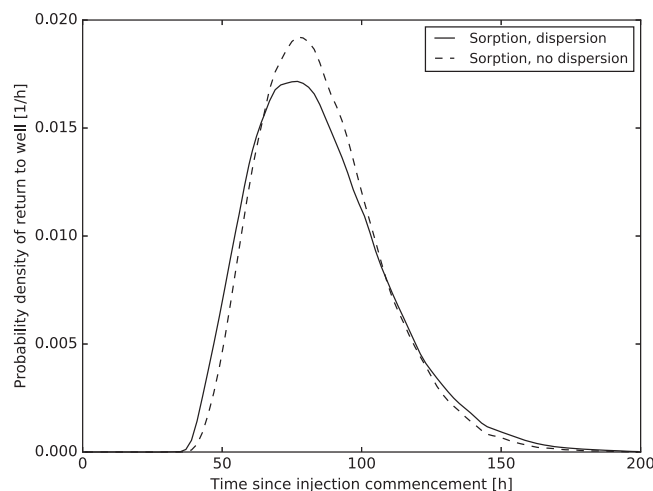
Figure 5. Comparison of breakthrough curves at well for push-pull test in heterogeneous media, with mobile-immobile (kinetic sorption) behavior, with and without pore-scale dispersion. The effect of pore-scale dispersion is seen in the difference between these curves.

Since local-scale dispersion and *K*-field heterogeneity affect the well breakthrough curve by inducing flow-line hysteresis (imperfect path reversibility), another instructive way to view the effect of these processes as they interact with mobile-immobile mass transfer is to examine the pathlines followed by distinct particles as they are tracked. In Figure 6, we show four scenarios: that of the canonical example, along with every other combination of local-scale dispersion and mobile-immobile mass transfer being turned on and off. The bottom two figures correspond to the two scenarios whose breakthrough curves are shown in Figure 5. Just how minor the hysteresis induced by pore-scale dispersion is may be surprising. In addition,
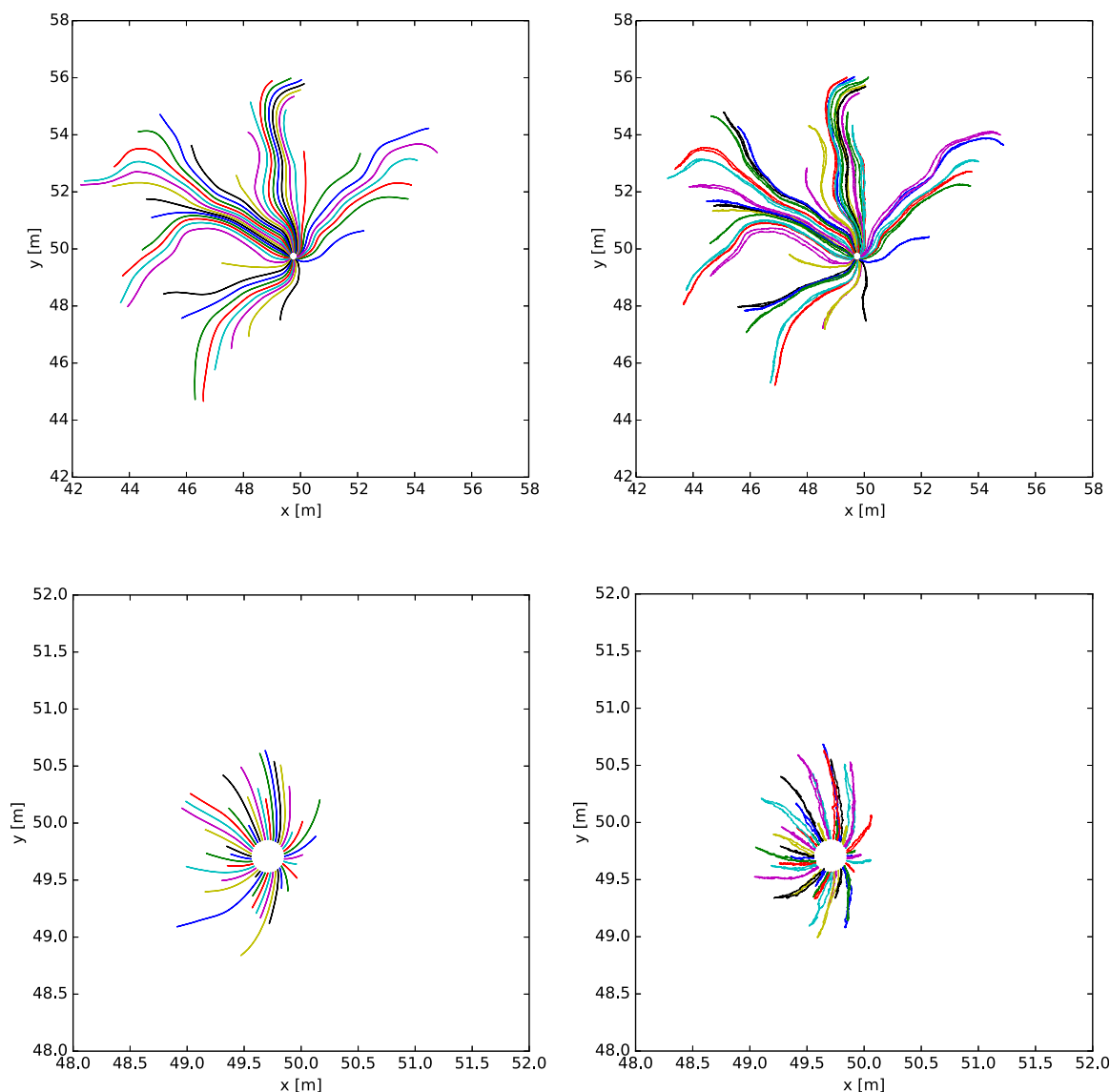
Figure 6. Outbound and inbound particle paths for 40 particles shown in map view over for variations on the canonical example. The top row features no mobile-immobile mass transfer, and the bottom row features mobile-immobile mass transfer as described in the canonical example (note different scales in each row). The left column features no local-scale dispersion, and the right column features local-scale dispersion as described in the canonical example. For additional clarity, the bottom left plot represents the exact conditions of the canonical example.

with strong trapping processes in effect, it is notable that the test interrogated only a cylinder with diameter of approximately 2 m, centered around the well. This illustrates that push-pull tests are plainly sensitive to local variabilities in immobilization properties, while being comparatively insensitive to flow-field heterogeneity.

4. Travel Time Analysis

4.1. Isochrones of the Pumping-Induced Flow Field

Consider the equal-time contours, or *isochrones*, of the flow field during the push phase. These are lines (or in 3-D systems, surfaces) which are reached in equal time by pure-advection along Darcy-scale streamlines. In a homogeneous domain, the isochrones will be perfect circles centered at the well (although not evenly spaced, as radial velocity decreases with distance from the well). In a heterogeneous domain, these will be irregularly-shaped, and be determined by the underlying hydraulic conductivity field. Figure 7 shows iso-chrones for both sorts of scenarios (the irregular isochrones correspond to the canonical example). If there were no trapping or other dispersive processes, a slug of solute introduced instantaneously would be
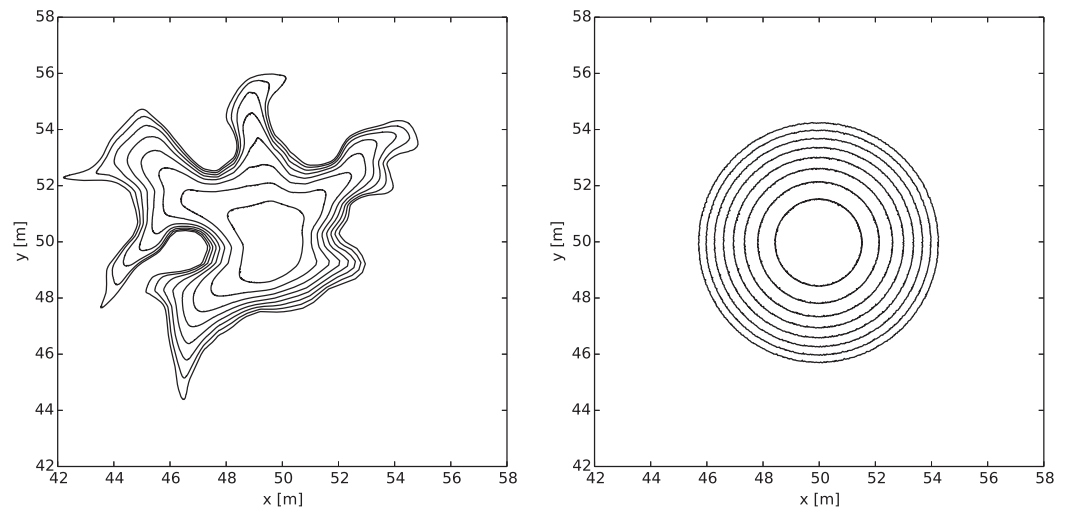
Figure 7. Isochrones displayed (in map view) at 5 h intervals from the beginning of the push phase. (left) Isochrones computed for the canonical example (with no local-scale dispersion). (right) Isochrones in homogeneous media corresponding to the same pumping rate and geometric mean conductivity.

uniformly distributed along a single isochrone after any given time, by definition. If the pumping rate were maintained but the pumping direction reversed then all of the tracer would arrive back at the well after the same amount of time over which pumping into the well took place (true for both sets of contours seen in Figure 7). Variability is only detectable to the extent that it causes solute to take an amount of time to complete the outbound trip from isochrone n to isochrone $n + 1$ that is different from the time taken to make the inbound trip from isochrone $n + 1$ back to isochrone n. This precludes the detection of flow field heterogeneity, except to the extent that the transport is hysteretic—with solute returning by a different path than that which it took on its outbound journey. Such insensitivity stands in striking contrast to the findings of *Pedretti et al.* [2013] regarding radially convergent tracer tests, namely that the primary cause of heavy-tailed breakthrough was flow field heterogeneity. To the extent that the effect of flow field heterogeneity may be neglected, and in the rest of the paper we shall assume it may be, push-pull tests isolate the temporal trapping effects of mobile-immobile processes, and are well positioned to quantify them. We demonstrate how this may be done below.

4.2. Isochrone First-Passage Times as Measures of Mobile-Immobile Mass Transfer

In contrast to classical push-pull analyses, which are continuum-based and rely on the ADE, our analysis employs the more general CTRW framework, which is capable of capturing behavior encoded by the ADE, as well as other behavior that it cannot capture. We employ CTRW ideas to conceptually discretize continuous solute motion as sequential transitions between the Darcy-scale isochrones introduced above, and then apply subordination theory to compute the CTRW transition distributions from the underlying physics.

The basic idea is to imagine an infinite set of isochrones with unit (temporal) spacing. An essential assumption is that whatever trapping process is driving the mobile-immobile behavior is spatially invariant, and everywhere is defined by the same capture rate per unit time, λ, and the same ψ_{im}. We recognize that this may be an idealization, as some systems may feature spatially-variable mass transfer properties whose scale of variability is large relative to the isochrone spacing, and these may in fact be correlated positively or negatively to the hydraulic conductivity field [*Allen-King et al.*, 2006]. Since a particle spends, by definition, unit time free while passing between isochrones, the probability distribution for transition between each successive pair of isochrones will be identical. The fundamental idea here is that individual CTRW transitions are *defined* as the space-time interval between first arrival at successive surfaces (with each adjacent pair having the same interarrival statistics). This is essentially the renewal plane CTRW (RP-CTRW) theory introduced previously by *Hansen and Berkowitz* [2014]. Here, however, the renewal "planes" that cause a transition to be registered are replaced by arbitrarily shaped successive isochrone surfaces. We thus transform a transport problem in a complex 2-D (or 3-D) flow field into a 1-D CTRW problem. Following the approach introduced by *Benson and Meerschaert* [2009], and also employed by *Dentz et al.* [2015], this distribution may be

computed by summing the product of the (Poisson-distributed) likelihood of k captures in unit time and the k-fold auto-convolution of ψ_{im}, for all k

$$\zeta_1(t) = \sum_{k=0}^{\infty} \frac{e^{-\lambda}\lambda^k}{k!}(\psi_{\mathrm{im}})^{*k}(t-1). \tag{7}$$

We can imagine that $\zeta_1(t)\,[\mathrm{T}^{-1}]$ represents a probabilistic mapping between a unit of time spent mobile (we will call this *operational time*) and an amount of total time (we will call this *clock time*). If $\lambda = 0$, then $\zeta_1(t) = \delta(t-1)$, and the operational and clock times are the same. More formally, we define the $\zeta(t; u)\,[\mathrm{T}^{-1}]$ to be the distribution function mapping between operational time, u, and clock time, t. $\zeta_1(t)$ and $\zeta(t; 1)$ are equivalent. Readers may note that $\zeta_1(t)$ is conceptually analogous to the $\psi(t)$ used in the RP-CTRW conceptualization. The change of notation is to avoid confusion with ψ_{m} and ψ_{im} used elsewhere in this paper.

Because the interarrival times for two pairs of isochrones are independent, it follows that $\zeta(t; 2) = \zeta(t; 1) * \zeta(t; 1)$, where $*$ denotes convolution. Define $\tilde{\zeta}(s; u) \equiv \mathcal{L}\{\zeta(t; u)\}$, denoting the $t \to s$ Laplace transform of $\zeta(t; u)$. (We will use an overbar tilde to denote $t \to s$ Laplace transformation.) In Laplace space, $\tilde{\zeta}(s; 2) = [\tilde{\zeta}_1(s)]^2$. We can see that this relationship extends to higher and fractional powers as well, and that in general,

$$\tilde{\zeta}(s; u) = [\tilde{\zeta}_1(s)]^u. \tag{8}$$

Given that $\zeta(t; u)$ represents the mapping from operational time to clock time, the following relation may be used to convert the particle arrival rate at location x in operational time, $R_{\mathrm{op}}(x, u)\,[\mathrm{T}^{-1}]$, to the particle arrival rate at x in clock time, $R_{\mathrm{cl}}(x, t)\,[\mathrm{T}^{-1}]$, where the symbol R has the same interpretation as in other CTRW literature [e.g., *Berkowitz et al.*, 2006]:

$$R_{\mathrm{cl}}(x, t) = \int_0^t \zeta(t; u)R_{\mathrm{op}}(x, u)\,du. \tag{9}$$

The validity of this relationship follows directly from viewing $\zeta(t; u)$ as the pdf for clock time, t, conditional on operational time, u, and noting that R_{op} and R_{cl} are proportional to first-passage time (operational and clock, respectively) pdfs at x. Thus, (9) is simply a marginalization integral for a conditional probability. By use of (8) and (9), we will show both that $\zeta_1(t)$ completely determines the breakthrough curve at the well (and is thus plausibly determinable via inverse analysis) and that it contains exactly the information needed to add mobile-immobile behavior into a transport model that only captures advective-dispersive behavior.

4.3. $\zeta_1(t)$ Determines the Push-Pull Breakthrough Curve

Imagine an isochronal coordinate system, written in terms of "spatial" coordinate $n\,[\mathrm{T}]$, instead of x, where this represents all locations that are accessible by a purely advective streamline-follower in *time n* during the push phase. (This is a continuum extension of the discrete isochrone picture illustrated in Figure 7.) This means that the n-coordinate of a particle at the end of the push phase represents the amount of time it was operational during that phase. Then by definition, $R_{\mathrm{op}}(n, t) = \delta(n-t)$. Using (9) with n replacing x, it follows that at the end of the push phase (time T_{push}), we have

$$R_{\mathrm{cl}}(n, T_{\mathrm{push}}) = \zeta(T_{\mathrm{push}}; n). \tag{10}$$

Breakthrough at the well will occur as soon as the particles have spent exactly as much time operational during the pull phase as they did during the push phase. Let $b(t)\,[\mathrm{T}^{-1}]$ be the probability distribution for the time taken by a particle between its initial departure from the well and its return. It follows that

$$b(t) = \int_0^{\infty} \zeta(T_{\mathrm{push}}; n)\zeta(t - T_{\mathrm{push}}; n)\,dn \quad t \geq T_{\mathrm{push}}. \tag{11}$$

By (8), the right-hand side is entirely determined by $\zeta_1(t)$, and by T_{push}, which is known. The flux concentration, $c_f\,[\mathrm{M\,L}^{-3}]$, at the well during the pull phase can then immediately be determined by taking the convolution of the flux concentration during the *push* phase with b

$$c_f(0, t) = \int_0^{T_{\mathrm{push}}} b(t-\tau)c_f(0, \tau)\,d\tau \quad t \geq T_{\mathrm{push}}. \tag{12}$$

Thus, we see that $\zeta_1(t)$ contains all the information about the subsurface that affects the breakthrough curve at the well.

4.4. $\zeta_1(t)$ Is Sufficient to Incorporate Mobile-Immobile Behavior Into a Transport Model

We assume that $R_{op}(x, u)$ has been previously determined for the relevant flow field, *excluding* mobile-immobile behavior. It will generally incorporate advection-driven anomaly that is invisible to a push-pull methodology, but in rare cases may be determined by the ADE. Noting that $\zeta(t; u) = 0$ for $u > t$, we can change the upper limit of integration from t to ∞, and then Laplace transform $t \rightarrow s$

$$\tilde{R}_{cl}(x, s) = \int_0^\infty \tilde{\zeta}(s; u) R_{op}(x, u) du. \tag{13}$$

We then apply (8) to show that

$$\tilde{R}_{cl}(x, s) = \int_0^\infty [\tilde{\zeta}_1(s)]^u R_{op}(x, u) du. \tag{14}$$

According to the analysis in *Benson and Meerschaert* [2009, equation (6)], if we have a mobile-immobile system in which the waiting time distribution for a single sojourn in the mobile phase, $\psi_m(t)$, is exponential with parameter λ (i.e., $\psi_m(t) = \lambda e^{-\lambda t}$), and the waiting time distribution for a single sojourn in the immobile phase, $\psi_{im}(t)$, is general, then we may write

$$[\tilde{\zeta}_1(s)]^u = e^{-u(s + \lambda[1 - \tilde{\psi}_{im}(s)])}. \tag{15}$$

Making the substitution $q \equiv s + \lambda[1 - \tilde{\psi}_{im}(s)]$ and substituting (15) into (14), we arrive at

$$\tilde{R}_{cl}(x, s) = \int_0^\infty e^{-qu} R_{op}(x, u) du, \tag{16}$$

where by definition, the right-hand side is just the $u \rightarrow q$ Laplace transform of $R_{op}(x, u)$, which we shall denote $\hat{R}_{op}(x, q)$. Then it follows from our definition of q that

$$\tilde{R}_{cl}(x, s) = \hat{R}_{op}(x, s + \lambda[1 - \tilde{\psi}_{im}(s)]) = \hat{R}_{op}(x, -\ln(\zeta_1(s))). \tag{17}$$

This is an especially opportune relationship, since if one works analytically in the CTRW paradigm to model the anomaly due to heterogeneous advection, then $\hat{R}_{op}(x, q)$ will usually, in any case, be obtained in the Laplace domain, and need numerical inversion. (Particle arrival rates can be translated into resident concentrations using methods outlined in *Berkowitz et al.* [2006, Appendix B].) In this case, adding additional anomaly due to mobile-immobile mass transfer (i.e., moving to clock time) to the anomaly owing to heterogeneous advection (modeled in operational time) does not add any complexity to the work flow.

An interesting aside at this point is how the analysis of mobile-immobile immobile mass transfer has illustrated the connections between the MRMT framework, as exemplified by (6), the RP-CTRW framework (ζ_1 conceived as an isochrone transition time), and the subordination theory (ζ_1 as defined in (7)).

4.5. Numerical Demonstration of Laplace-Domain ζ_1 Substitution

To demonstrate our technique, we return to the canonical example. We use the heterogeneous conductivity field and mass transfer parameters used there, but alter the boundary conditions defining the flow field. In particular, we simulate steady-state flow in this domain under strong advection using PFLOTRAN, applying a left-to-right head drop of 10.4 m and applying no-flow boundaries on the other two faces. (The large gradient increases the speed of the particle tracking algorithm when sorption is turned on, and is immaterial for the purposes of our demonstration.) The resulting flow field is shown in Figure 8. In this flow field, we perform two particle tracking simulations, both beginning with particles initially uniformly distributed along the left edge of the domain. The demonstration procedure is this:

1. 50,000 particles are released, and passively follow the flow lines. The time of arrival at the right edge of the domain is recorded for each particle and a histogram is produced, representing the downgradient breakthrough curve, $R_{op}(t)$. This is shown in the top plot of Figure 9.
2. 10,000 particles are released, and follow the flow lines, but subject to periodic trapping and release governed by the same λ and μ that were used in the canonical example. A second histogram is produced, representing another particle breakthrough curve, $R_{cl}(t)$.
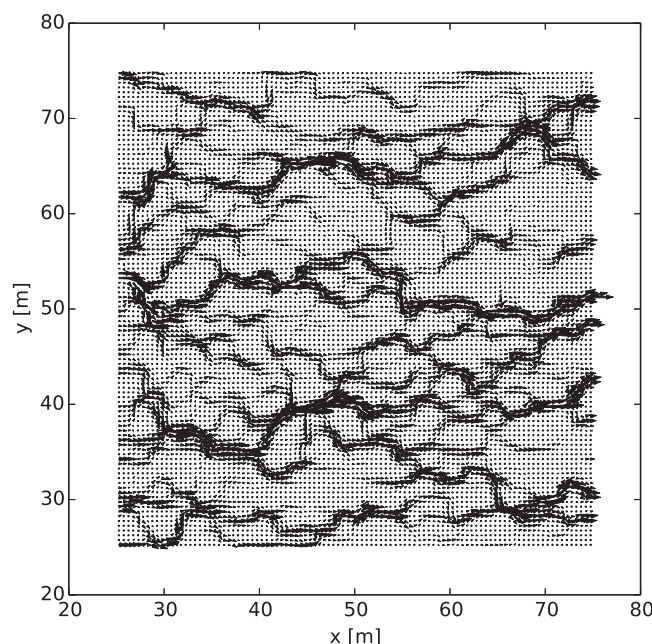
Figure 8. Map of flow induced by a left-to-right hydraulic head drop of 0.2 m, imposed on the same heterogeneous conductivity field shown in Figure 4. No-flow boundary conditions were imposed at the top and bottom of the domain.

3. The Laplace transform of the breakthrough curve generated in point 1 is numerically computed, the substitution (17) is applied (with ζ_1 related to λ and μ via (7), and the Laplace transform is numerically inverted to generate a prediction of the breakthrough curve generated in point 2.

The breakthrough curves generated in steps 2 and 3, respectively, are shown on the bottom plot of Figure 9. The high degree of coherence between these two curves demonstrates the validity of the relation summarized in (17).

5. Monte Carlo Parameter Identification and Further Informational Limitations of Push-Pull Tests

In light of the above analysis, we are motivated to determine $\zeta_1(t)$ from the push-pull breakthrough curve, so that we may apply it to predict transport under linear flow in the same domain. Such breakthrough curve interpretation is an inverse problem. The unknown ζ_1 (along with known parameters, such as pumping rate and duration) determines completely the observed breakthrough curve at the well. It is natural to attempt invert this by a minimum-residual technique: knowing the well breakthrough curve, we seek to determine $\zeta_1(t)$ by selecting definitions at random and choosing the one that best recreates the breakthrough curve. In developing algorithms for this purpose, we will come to see another feature that is largely or totally invisible to push-pull tests beyond those identified in section 3.

5.1. Direct Monte Carlo Solution for ζ_1
The following is a straightforward, flow-field-agnostic approach to the problem of identifying ζ_1, based on subordination ideas (for simplicity, we assume that Q_{in} and Q_{ex} are the same):

1. Generate initial guess for ζ_1.
2. For each of a number of iterations:
   a. For each of a large number of particles:
      i. Initialize two variables, $T_{cl}=0$, and $T_{op}=0$, reflecting, respectively, the particle's clock and operational time.
      ii. For the push phase: while T_{cl} is less than the end time of the push phase, use a pseudo-random number generator to repeatedly generate samples from the distribution ζ_1. For each sample, Z, increment $T_{cl}=0$, and $T_{op}=0$ by Z.
      iii. For the pull phase: while $T_{op} > 0$ repeatedly generate samples from the distribution ζ_1. Increment T_{cl} by Z, and decrement T_{op} by Z.
      iv. Record the final T_{cl} corresponding to $T_{op}=0$ (i.e., breakthrough back at the well).
   b. Generate a histogram from the final T_{cl} for each particle.
   c. Compute the L2 norm of the difference between the histogram generated and the breakthrough curve at the well.
   d. If this is the smallest L2 norm yet seen, set "variable" $\zeta_1^{best}=\zeta_1$.
3. Return ζ_1^{best}.

5.2. Indirect Monte Carlo Solution for ζ_1 by Means of λ and ψ_{im}

We might instead attempt to solve directly for λ and ψ_{im}, the determinants of ζ_1 per (7), and of general transport behavior per (6 or 17). The following algorithm does this, also allowing for a potential pause between push and pull phases, and differential pumping rates during the push and pull phases.

1. Generate initial guesses for λ (defining the exponential ψ_m) and ψ_{im}.
2. For each of a number of iterations:
   a. For each of a large number of particles:
      i. Initialize two variables, $T_{cl}=0$, and $T_{op}=0$, reflecting, respectively, the clock and operational times of the particle.
      ii. While T_{cl} is less than the end time of the push phase:
         A. Draw a sample from the distribution ψ_m. Add this to both T_{cl}, and T_{op}.
         B. Skip directly to next phase (pause or pull) if T_{cl} is greater than the length of the push phase.
         C. Draw a sample from the distribution ψ_{im}. Add this to T_{cl} alone.
      iii. While T_{cl} is less than the end time of the pause phase (if any):
         A. Draw a sample from the distribution ψ_m. Add this to both T_{cl} alone.
         B. Skip to pull phase if T_{cl} is greater than the end time of the pause phase.
         C. Draw a sample from the distribution ψ_{im}. Add this to T_{cl}.
      iv. While $T_{op} > 0$ (pull phase):
         A. Draw a sample from the distribution ψ_m. Add this to T_{cl}, and subtract* this from T_{op}.
         B. End pull phase immediately if $T_{op} \leq 0$.
         C. Draw a sample from the distribution ψ_{im}. Add this to T_{cl}.
      v. Record the final T_{cl} corresponding to $T_{op}=0$ (i.e., breakthrough back at the well).
   b. Generate a histogram from the final T_{cl} for each particle.
   c. Compute the L2 norm of the difference between the histogram generated and the breakthrough curve at the well.
   d. If this is the smallest L2 norm yet seen, set "variables" $\lambda^{best}=\lambda$ and $\psi_{im}^{best}=\psi_{im}$.
3. Return λ^{best} and ψ_{im}^{best}.

*If $Q_{in} \neq Q_{ex}$ during the pull phase, sample $t \sim \psi_m$ as before but instead subtract $t\frac{Q_{ex}}{Q_{in}}$ from T_{op}.
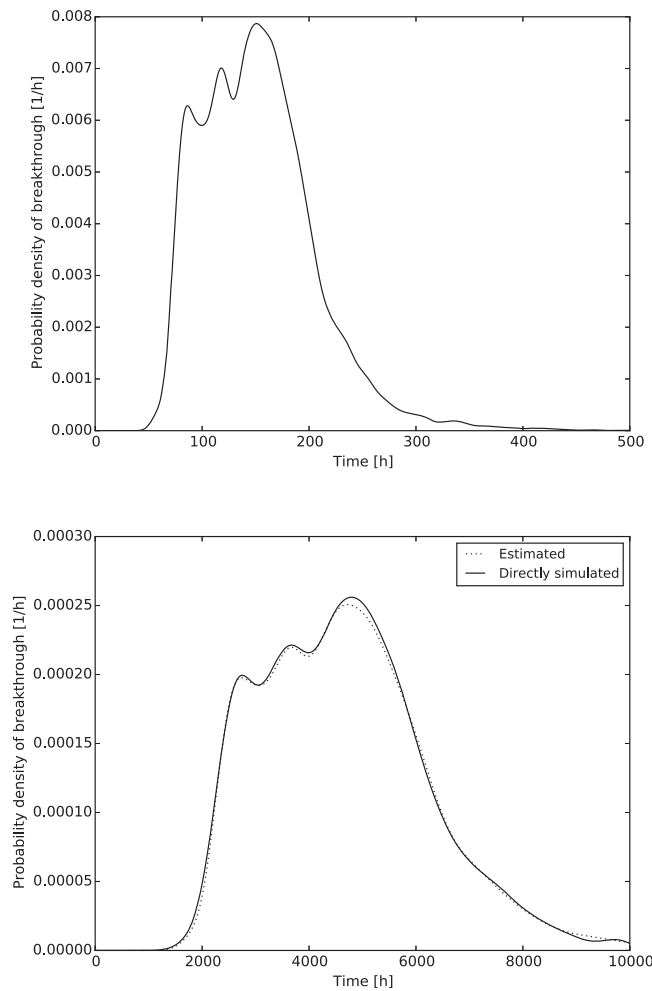
5.3. Informational Limitations

It is unfortunately not possible to determine ζ_1 *uniquely* by using the direct algorithm of section 5.1. To see this, imagine the following scenario: We pick a random parameterization we hope represents $\zeta_1(t)$. However, unbeknownst to us, we have actually picked the parameterization representing $\zeta(t; 2)$. For each particle, we repeatedly draw from this distribution and add it to the clock time (adding one to the operational time on each draw, instead of two, which would be correct) until the length of the push phase is over. We then repeat the process for the pull phase, subtracting one instead of two. Since the operational time is incremented and then decremented by the same multiplier, it reaches zero after the same number of transitions as if the multiplier were unity. Thus, we will also generate the correct breakthrough curve by this method, and we cannot distinguish between different members of the family $\zeta(t; u)$ by Monte Carlo analysis. If $\zeta_1(t)$ has a power-law tail, and one is only interested in characterizing its exponent, β, then selection of any member of the family $\zeta(t; u)$ should be sufficient, as all will share the same β. However, this is not sufficient for predictive modeling. Note that since $\zeta_1(t)$ is both the sole functional determinant of the breakthrough curve, and contains exactly the information required for predictive modeling, this represents a limitation of the push-pull test methodology, not this particular interpretive method.

We will now demonstrate that the impossibility of unique identification of ζ_1 may be attributed to lack of sensitivity of the well breakthrough curve to the capture probability, λ. Combining (8) and (15) and explicitly writing λ as a parameter yields

$$\tilde{\zeta}(s; u, \lambda)=e^{-(us+\lambda u[1-\bar{\psi}_{im}(s)])}, \tag{18}$$

which can be rewritten as

$$\tilde{\zeta}(s; u, \lambda) = e^{-(u-1)s}e^{-(s+\lambda u[1-\bar{\psi}_{im}(s)])}.$$

(19)

Determining the inverse Laplace transform, it follows that

$$\zeta(t-(u-1); u, \lambda) = \zeta(t; 1, \lambda u).$$ (20)

We established immediately above that breakthrough curves drawn from $\zeta(t; u, \lambda)$ and $\zeta(t; 1, \lambda)$ are not distinguishable by Monte Carlo analysis. We will use the relational operator $\bowtie$ to indicate distributions that cannot be distinguished by push-pull analysis, so $\zeta(t; u, \lambda) \bowtie \zeta(t; 1, \lambda)$.

Consider two values, u_1 and u_2, arbitrary save for the constraints $u_1 \ll 1$ and $u_2 \ll 1$. Then by (20),

$$\zeta(t; 1, \lambda u_1) \approx \zeta(t+1; u_1, \lambda)$$
$$\bowtie \zeta(t+1; 1, \lambda),$$ (21)
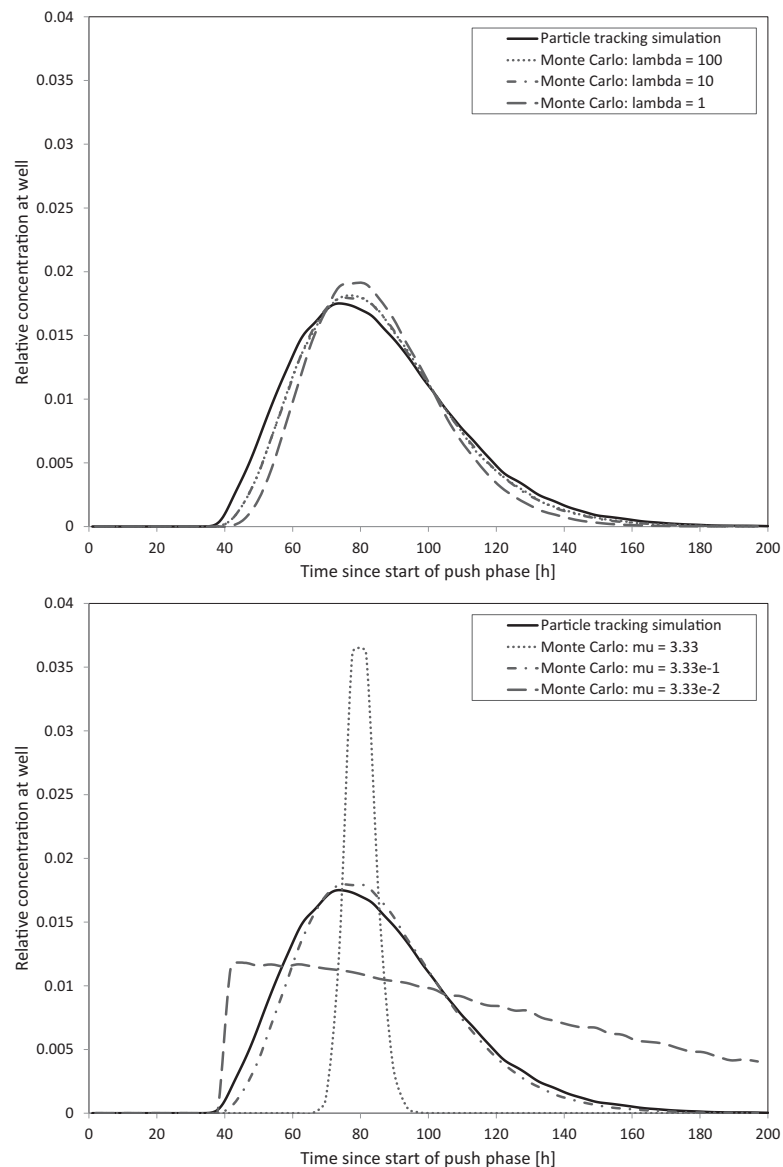
and similarly,

$$\zeta(t; 1, \lambda u_2) \approx \zeta(t+1; u_2, \lambda)$$
$$\bowtie \zeta(t+1; 1, \lambda).$$ (22)

Defining $\lambda_1 \equiv \lambda u_1$ and $\lambda_2 \equiv \lambda u_2$,

$$\zeta(t; 1, \lambda_1) \bowtie \zeta(t; 1, \lambda_2).$$ (23)

Since in this analysis λ can have any magnitude, λ_1 and λ_2 are arbitrary. This analysis shows mathematically, and for arbitrary ψ_{im}, push-pull testing will be largely unresponsive to the capture rate, λ, which we observed for

Figure 9. (top) Directly simulated breakthrough curve or left-to-right transit times in the flow field illustrated in Figure 8, with no mobile-immobile mass transfer. (bottom) Comparison of breakthrough curves for the same scenario but with mobile-immobile mass transfer, as computed directly by particle tracking (solid curve), and by applying relation (17) to the pdf shown on the top plot (dashed curve). NB: Axes on the two subplots have different scales.

exponential ψ_{im} in section 3.2. The variations in the breakthrough curves we then are justified in attributing to variation in ψ_{im}. This lack of sensitivity to λ is inherent in a push-pull test methodology, not an artifact of the interpretation scheme.

5.4. Numerical Demonstration

Presently, we give a twofold demonstration. In particular, we seek to show:

1. That the breakthrough curve found using the indirect Monte Carlo algorithm matches the "true" breakthrough curve generated by particle tracking, if seeded with the correct λ and ψ_{im}.
2. That the breakthrough curve at the well is insensitive to λ and sensitive to ψ_{im}.

We return for a final time to the canonical example. We demonstrate our first point by running the indirect Monte Carlo algorithm through once (i.e., running the outer loop once, without guessing new sets of parameters), initially seeded with the same mass transfer parameters used in the canonical example (recall that in that example, ψ_{im} is exponential with parameter $\mu = \frac{1}{3}$ h^{-1}, and $\lambda = 10$ h^{-1}). It is seen in the upper plot of Figure 10, that there is a solid match between breakthrough curves generated by particle tracking on the full velocity field in section 3.3 and by the purely temporal, subordination-based Monte Carlo algorithm of section 5.2.

Figure 10. Illustration of the respective impact of changes in λ and changes in μ on Monte Carlo-predicted breakthrough curves, versus the "true" breakthrough curve from the canonical example. (top) The Monte Carlo algorithm was run for values of λ varying over three orders of magnitude (the middle value being correct), and μ held steady at the correct value. (bottom) The Monte Carlo algorithm was run for values of μ varying over three orders of magnitude (the middle value being correct), and λ held steady at the correct value.

The second point is also illustrated in the same figure. On the upper plot, the results of running the Monte Carlo algorithm once, with values of λ perturbed by an order of magnitude in both directions are shown; it is apparent that this has a negligible effect on the final anticipated breakthrough curve. On the lower plot, λ is fixed at the correct value, with values of μ perturbed by an order of magnitude in both directions. The profound effect on the observed breakthrough curve is visible. We thus corroborate the argument that the well breakthrough curve is sensitive to ψ_{im} (meaning in this case, μ), but insensitive to λ.

6. Analysis of MADE Site Push-Pull Test

Previously, our analysis has been performed on a synthetic push-pull test, with exponentially distributed ψ_{im}. To conclude the presentation, we now demonstrate our Monte Carlo parameterization scheme on data from a real
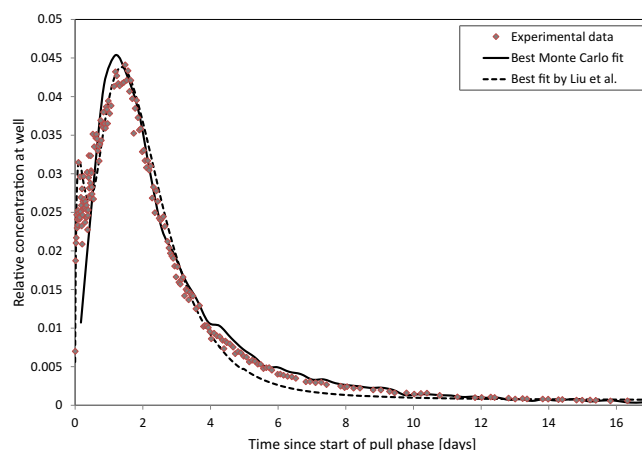
Figure 11. Comparison of experimental measurements at the MADE site push-pull tracer test with the best fit breakthrough curve predicted by our algorithm, and the closest-fitting 3-D numerical model in *Liu et al.* [2010].

push-pull test, one for which a nonexponential $\psi_{im}(t)$ is appropriate. The test was performed by *Liu et al.* [2010] at the well-known MADE site, which is a multiple-porosity, heterogeneous hydraulic conductivity site. This test thus represents a suitable one for our theory.

The push-pull test we modeled is carefully described by *Liu et al.* [2010]. The parameters that are relevant to our modeling are summarized here: the push phase lasted for 26.75 h (the injection contained solute for the first 4.1 h, followed by native water for the rest of the phase), with $Q_{in}=8.18\,\mathrm{m^3\,d^{-1}}$. Pumping was halted for 18.7 h. Finally, the pull phase took place for 410.3 h, with $Q_{ex}=7.90\,\mathrm{m^3\,d^{-1}}$.

The test was successfully modeled by Liu et al. by fitting a high resolution (over 10^7 cell) 3-D numerical flow and transport model, where three irregularly shaped zones of varying hydraulic conductivity were populated by means of extensive direct-push measurements in the vicinity of the test well. In addition to the detailed, irregular hydraulic conductivity field, their model contained six tunable transport parameters (three dispersivities, total porosity and two directly describing the mobile-immobile process), three of which were pre-populated by other testing at the site. The other three parameters were calibrated from the push-pull test data, resulting in the fit shown in Figure 11.

We fit the same data by use of the Monte Carlo technique outlined in section 5. For simplicity, we assume an instantaneous release of solute at $T_{cl}=T_{op}=0$, as contrasted with the nonnegligible time of solute injection in the actual push-pull test. (This may be a cause of the slight divergence from measured concentrations seen at very early time in Figure 11.) We also assume that $\psi_{im}(t)$ has the form of a truncated power law (TPL), which is a heavy-tailed distribution with exponential tempering at late time. It is defined [*Berkowitz et al.*, 2006] by three parameters, t_1 [T], t_2 [T], and β. As usual, $\psi_m(t)$, is taken as exponential, defined by λ. Thus, we are faced with a four-parameter inverse problem. Our best fit is also shown in Figure 11. This fit corresponds to parameters $t_1=0.0173$ d, $t_2=12.2$ d, and $\beta=0.71$, which represents highly anomalous transport. CTRW models of realistic transport commonly employ values of $\beta > 1$ (larger values, all else being equal, indicate quicker late-time approach to the Fickian regime). Given the magnitude of t_2 (which may be thought of as the onset time for late-time exponential tempering), we see that this is reflected in the breakthrough curve tail, but does not affect the essential power-law nature of ζ_1.

It may be initially surprising to see that the quality of fit obtained by our simple four-parameter scheme is comparable to the quality of fit obtained by a detailed 3-D numerical model. However, the insight that we derive from the isochrone conception is that the K-field variability is essentially invisible to a push-pull methodology. A useful implication of these results is that there appears to be no need for complex 3-D numerical models to interpret push-pull data, as their parameters will be not constrained by the data. Since both models calibrate mobile-immobile trapping with exponential $\psi_m(t)$, it is perhaps not surprising that they give similar quality results. We consider that the excellent fit seen here provides practical corroboration for the theory developed above.

7. Summary and Conclusions

We analyzed the nature of the path reversibility assumption that underpins much of the push-pull interpretation literature by means of a parametric study. We quantified the combined scattering effect of ambient drift, local-scale dispersion, and K-field heterogeneity, and compared it with the scattering effect of mobile-immobile mass transfer. We identified a region of the parameter space in which path reversibility could be unproblematically assumed while attributing the push-pull breakthrough curve behavior to

mobile-immobile mass transfer. We then presented a new conceptual model, based on travel time pdf's, for the interpretation of push-pull tracer tests to quantify mobile-immobile behavior, alongside a Monte Carlo technique for solving the parametric inverse problem by iteratively generating breakthrough curves in using an efficient subordination-based scheme. Our conceptual scheme avoided making assumptions about the spatial homogeneity of the flow field; only about the homogeneity of the mass transfer processes. The mobile-immobile system is considered to be spatially homogeneous, with mobile solute subject to probability of immobilization per unit time λ and the length of single immobilization event to be drawn from pdf ψ_{im}. The interpretation methodology is based on the calibration of $\zeta_1(t)$, the probability distribution function for the time taken to transition between isochrones (equal-arrival-time contours) of Darcy flow with unit-time spacing. This function was seen to uniquely determine the breakthrough curve at the well, and to provide enough information to add mobile-immobile behavior into other transport models, using an elegant transformation in the Laplace domain. Analyzing nonuniqueness, it was seen that additional information, besides that available from the push-pull test, is needed for predictive modeling.

We summarize here the key conclusions arising from the ideas and numerical experiments considered above:

1. Contrary to common assumption, path reversibility is not assured in push-pull tests. Only for sufficiently slow remobilization processes will scattering in the well return time (i.e., breakthrough) pdf, $b(t)$, due to mobile-immobile mass transfer predominate over that due to pathline hysteresis (caused by hydrodynamic factors such as local-scale dispersion and ambient drift).
2. For ψ_{im} with large mean, we justified the idealization that the push-pull breakthrough curve is affected only by mobile-immobile mass transfer and contains no information about drift and local-scale dispersion.
3. If there is no local-scale dispersion or ambient drift (path reversibility idealization), the pdf $\zeta_1(t)$ entirely determines the push-pull breakthrough curves. It can also, regardless of drift velocity, be employed to directly incorporate mobile-immobile mass transfer into any advective transport model. $\zeta_1(t)$ can be viewed in two different ways: as a single CTRW transition distribution in the RP-CTRW framework, or as a subordinator in the subordination framework, highlighting the connection between the approaches in the context of mobile-immobile mass transfer.
4. Assuming solute path reversibility, push-pull tests were seen to reveal *nothing* spatial. Not only is irregular isochrone shape essentially invisible, so too is the spatial scale. If the units of the plots in Figure 7 were instead cm or km, but the corresponding $\zeta_1(t)$ functions were unchanged, the same breakthrough curve would be observed at the well.
5. A corollary of this is that the radial flow-field symmetry idealizations commonly used in push-pull test interpretation are harmless to the extent that the path-reversibility idealizations are harmless.
6. It was seen impossible to identify $\zeta_1(t)$ from a family of functions $\zeta(t; u)$. If ψ_{im} has a power-law tail, implying that $\zeta_1(t)$ has one also, and if one is interested in its exponent (as the determinant of the nature of the anomalous transport), then this may be sufficient, since all members of the family have the same power-law tail. However, direct fitting of ζ_1 does not enable predictive modeling.
7. The possibility of *directly* computing the underlying $\psi_{im}(t)$, by a subordination-based Monte Carlo technique that involved *only* temporal variables, was demonstrated. However, the immobilization rate, λ, must be estimated by other means; it is not identifiable by a push-pull methodology.
8. The Monte Carlo techniques were shown applicable to real data from a push-pull experiment in a highly heterogeneous aquifer at the MADE site. Our Monte Carlo method was seen to perform as well as direct simulation using an elaborate 3-D numerical model with explicitly modeled zones of different hydraulic conductivity. The travel time/isochrone theory, which implies the invisibility of large-scale heterogeneity, explains this perhaps surprising result.
9. Assuming $\zeta_1(t)$ has been correctly identified, a mathematical formula allows incorporation of mobile-immobile behavior into transport models encoding advective-dispersive effects only.

A possibly important direction for future research is further investigation of the information content of the push-pull test. How rich a family of functions ψ_{im} can we characterize, to what degree of uncertainty, and what are the implications of this uncertainty for model predictions related to contaminant transport under general flow conditions (different from the push-pull-test flow configuration)? It is also important to develop means to characterize the immobilization rate, λ, simply and reliably.

References

Allen-King, R. M., D. P. Divine, M. J. L. Robin, J. R. Alldredge, and D. R. Gaylord (2006), Spatial distributions of perchloroethylene reactive transport parameters in the borden aquifer, *Water Resour. Res.*, *42*, W01413, doi:10.1029/2005WR003977.

Benson, D. A., and M. M. Meerschaert (2009), A simple and efficient random walk solution of multi-rate mobile/immobile mass transport equations, *Adv. Water Resour.*, *32*(4), 532–539, doi:10.1016/j.advwatres.2009.01.002.

Berkowitz, B., A. Cortis, M. Dentz, and H. Scher (2006), Modeling non-Fickian transport in geological formations as a continuous time random walk, *Rev. Geophys.*, *44*, RG2003, doi:10.1029/2005RG000178.

Boisson, A., P. de Anna, O. Bour, T. Le Borgne, T. Labasque, and L. Aquilina (2013), Reaction chain modeling of denitrification reactions during a push–pull test, *J. Contam. Hydrol.*, *148*, 1–11, doi:10.1016/j.jconhyd.2013.02.006.

Borowczyk, M., J. Mairhofer, and A. Zuber (1967), Single well pulse technique, in *Isotopes in Hydrology*, International Atomic Energy Agency, Vienna.

Cassiani, G., L. F. Burbery, and M. Giustiniani (2005), A note on in situ estimates of sorption using push-pull tests, *Water Resour. Res.*, *41*, W03005, doi:10.1029/2004WR003382.

Dentz, M., P. K. Kang, and T. Le Borgne (2015), Continuous time random walks for non-local radial solute transport, *Adv. Water Resour.*, *82*, 16–26, doi:10.1016/j.advwatres.2015.04.005.

Doughty, C. (2010), Analysis of three sets of SWIW tracer-test data using a two-population complex fracture model for matrix diffusion and sorption, *Tech. Rep.* LBNL-3006E, Lawrence Berkeley Natl. Lab., Berkeley, Calif.

Drazer, G., M. Rosen, and D. H. Zanette (2000), Anomalous transport in activated carbon porous samples: Power-law trapping-time distributions, *Physica A*, *283*(1–2), 181–186, doi:10.1016/S0378-4371(00)00149-7.

Fetter, C. W. (1999), *Contaminant Hydrogeology*, Prentice Hall, Upper Saddle River, N. J.

Gelhar, L. W., and M. A. Collins (1971), General analysis of longitudinal dispersion in nonuniform flow, *Water Resour. Res.*, *7*(6), 1511–1521, doi:10.1029/WR007i006p01511.

Gouze, P., T. Le Borgne, R. Leprovost, G. Lods, T. Poidras, and P. Pezard (2008a), Non-Fickian dispersion in porous media: 1. Multiscale measurements using single-well injection withdrawal tracer tests, *Water Resour. Res.*, *44*, W06426, doi:10.1029/2007WR006278.

Gouze, P., Y. Melean, T. Le Borgne, M. Dentz, and J. Carrera (2008b), Non-Fickian dispersion in porous media explained by heterogeneous microscale matrix diffusion, *Water Resour. Res.*, *44*, W11416, doi:10.1029/2007WR006690.

Haggerty, R., and S. M. Gorelick (1995), Multiple-rate mass transfer for modeling diffusion and surface reactions in media with pore-scale heterogeneity, *Water Resour. Res.*, *31*(10), 2383–2400, doi:10.1029/95WR10583.

Haggerty, R., M. H. Schroth, and J. D. Istok (1998), Simplified method of ''Push-Pull'' test data analysis for determining in situ reaction rate coefficients, *Ground Water*, *36*(2), 314–324.

Haggerty, R., S. W. Fleming, L. C. Meigs, and S. A. McKenna (2001), Tracer tests in a fractured dolomite: 2. Analysis of mass transfer in single-well injection-withdrawal tests, *Water Resour. Res.*, *37*(5), 1129–1142.

Hansen, S. K. (2015), Effective ADE models for first-order mobile-immobile solute transport: Limits on validity and modeling implications, *Adv. Water Resour.*, *86*, 184–192, doi:10.1016/j.advwatres.2015.09.011.

Hansen, S. K., and B. Berkowitz (2014), Interpretation and nonuniqueness of CTRW transition distributions: Insights from an alternative solute transport formulation, *Adv. Water Resour.*, *74*, 54–63, doi:10.1016/j.advwatres.2014.07.011.

Huang, J., J. A. Christ, and M. N. Goltz (2010), Analytical solutions for efficient interpretation of single-well push-pull tracer tests, *Water Resour. Res.*, *46*, W08538, doi:10.1029/2008WR007647.

Kang, P. K., T. Le Borgne, M. Dentz, O. Bour, and R. Juanes (2015), Impact of velocity correlation and distribution on transport in fractured media: Field evidence and theoretical model, *Water Resour. Res.*, *51*, 940–959, doi:10.1002/2014WR015799.

Larsson, M., C. Doughty, C.-F. Tsang, and A. Niemi (2013), Understanding the effect of single-fracture heterogeneity from single-well injection-withdrawal (SWIW) tests, *Hydrogeol. J.*, *21*(8), 1691–1700, doi:10.1007/s10040-013-0988-x.

Lessoff, S., and L. Konikow (1997), Ambiguity in measuring matrix diffusion with single-well injection/recovery tracer tests, *Groundwater*, *35*(1), 166–176.

Lichtner, P. C., G. E. Hammond, C. Lu, S. Karra, G. Bisht, B. Andre, R. T. Mills, and J. Kumar (2015), PFLOTRAN user manual: A massively parallel reactive flow and transport model for describing surface and subsurface processes, *Tech. Rep. LA-UR-15-20403*, Los Alamos Natl. Lab., Los Alamos, N. M.

Liu, G., C. Zheng, G. R. Tick, J. J. Butler, and S. M. Gorelick (2010), Relative importance of dispersion and rate-limited mass transfer in highly heterogeneous porous media: Analysis of a new tracer test at the Macrodispersion Experiment (MADE) site, *Water Resour. Res.*, *46*, W03524, doi:10.1029/2009WR008430.

Mackay, D. M., D. L. Freyberg, P. V. Roberts, and J. A. Cherry (1986), A natural gradient experiment on solute transport in a sand aquifer: 1. Approach and overview of plume movement, *Water Resour. Res.*, *22*(13), 2017–2029, doi:10.1029/WR022i013p02017.

Margolin, G., M. Dentz, and B. Berkowitz (2003), Continuous time random walk and multirate mass transfer modeling of sorption, *Chem. Phys.*, *295*(1), 71–80, doi:10.1016/j.chemphys.2003.08.007.

Mercado, A. (1966), Underground water storage study: Recharge and mixing tests at Yavne 20 well field, *Tech. Rep. 12*, TAHAL - Water Planning for Israel Ltd., Tel Aviv, Israel.

Michalak, A. M., and P. K. Kitanidis (2000), Macroscopic behavior and random-walk particle tracking of kinetically sorbing solutes, *Water Resour. Res.*, *36*(8), 2133–2146, doi:10.1029/2000WR900109.

Neretnieks, I. (2007), Single well injection withdrawal tests (SWIW) in fractured rock: Some aspects on interpretation, *Tech. Rep. R-07-54*, Svensk Kärnbränslehantering AB, Stockholm.

Nordqvist, R., and E. Gustafsson (2002), Single-well injection-withdrawal tests (SWIW): Literature review and scoping calculations for homogeneous crystalline bedrock conditions, *Tech. Rep.* SKB- R-02-34, Swedish Nuclear Fuel and Waste Management Co., Stockholm, Sweden.

Nordqvist, R., and E. Gustafsson (2004), Single-well injection-withdrawal tests (SWIW): Investigation of evaluation aspects under heterogeneous crystalline bedrock conditions, *Tech. Rep.* SKB- R-04-57, Swedish Nuclear Fuel and Waste Management Co., Stockholm, Sweden.

Pedretti, D., D. Fernandez-Garcia, D. Bolster, and X. Sanchez-Vila (2013), On the formation of breakthrough curves tailing during convergent flow tracer tests in three-dimensional heterogeneous aquifers, *Water Resour. Res.*, *49*, 4157–4173, doi:10.1002/wrcr.20330.

Salamon, P., D. Fernandez-Garcia, and J. J. Gomez-Hernandez (2006), Modeling mass transfer processes using random walk particle tracking, *Water Resour. Res.*, *42*, W11417, doi:10.1029/2006WR004927.

Schroth, M. H., and J. D. Istok (2006), Models to determine first-order rate coefficients from single-well push-pull tests, *Ground Water*, *44*(2), 275–283, doi:10.1111/j.1745-6584.2005.00107.x.

Schroth, M. H., J. D. Istok, and R. Haggerty (2000), In situ evaluation of solute retardation using single-well push-pull tests, *Adv. Water Resour.*, *24*, 105–117, doi:10.1016/S0309-1708(00)00023-3.

Schroth, M. H., J. Kleikemper, C. Bolliger, S. M. Bernasconi, and J. Zeyer (2001), In situ assessment of microbial sulfate reduction in a petroleum-contaminated aquifer using push-pull tests and stable sulfur isotope analyses, *J. Contam. Hydrol.*, *51*(3–4), 179–195, doi: 10.1016/S0169-7722(01)00128-0.

Schulze-Makuch, D. (2005), Longitudinal dispersivity data and implications for scaling behavior, *Ground Water*, *43*(3), 443–456, doi:10.1111/j.1745-6584.2005.0051.x.

Snodgrass, M. F., and P. K. Kitanidis (1998), A method to infer in situ reaction rates from push-pull experiments, *Ground Water*, *36*(4), 645–650.

Tsang, Y. W. (1995), Study of alternative tracer tests in characterizing transport in fractured rocks, *Geophys. Res. Lett.*, *22*(11), 1421–1424, doi:10.1029/95GL01093.